Title

Stable Luminous Nanocomposites of Confined Mn2+-Doped Lead Halide Perovskite Nanocrystals in Mesoporous Silica Nanospheres as Orange Fluorophores

Journal

Inorganic Chemistry, 58(6)

ISSN

0020-1669

Authors

Pan, Aizhao

Wu, Youshen

Yan, Ke

et al.

Publication Date

2019-03-18

DOI

10.1021/acs.inorgchem.9b00010

Peer reviewed

Stable Luminous Nanocomposites of Confined Mn^{2+} Doped Lead Halide Perovskite Nanocrystals in Mesoporous Silica Nanospheres as Orange Fluorophores

Aizhao Pan,[,†] Youshen Wu,[†] Ke Yan,[$] Yun Yu,[†] Matthew J. Jurow,[‡,#] Baoyi Ren,[‡,&,] Cong Zhang,[‡] Shujiang Ding,[†] Ling He,[*,†] and Yi Liu[*,‡,#]*

[†] Department of Chemistry, School of Science, Xi'an Jiaotong University, Xianning West Road, 28, Xi'an, 710049, China.

[$] Key Laboratory of Education Ministry for Modern Design and Rotor-Bearing System, Xi'an Jiaotong University, Xi'an 710049, China.

[‡] The Molecular Foundry and [#] Materials Sciences Division, Lawrence Berkeley National Laboratory, Berkeley, California 94720, United States.

[&] Key Laboratory of Inorganic Molecule-Based Chemistry of Liaoning Province, College of Applied Chemistry, Shenyang University of Chemical Technology, Shenyang, 110142, China.

ABSTRACT

Creating highly stable inorganic perovskite nanocrystals ($CsPbX_3$, X=Cl, Br and I) with excellent optical performance is challenging because their optical properties depend on their ionic structure and its inherent defects. Here, we present a facile and effective synthesis using a nano-confinement strategy to grow Mn^{2+}-doped $CsPbCl_3$ nanocrystals embedded in dendritic mesoporous silica nanospheres (MSNs). The resulting nanocomposite is abbreviated as $Cs(Pb_x/Mn_{1-x})Cl_3$@MSNs and can serve as the orange emitter for white light-emitting diodes (WLED). The MSN matrix was prepared via a templated *sol-gel* technique as monodispersed center-radial dendritic porous particles, with a diamater of around 105 nm and an inner pore size of around 13 nm. The MSN was then utilized as the matrix to initiate the growth of Mn-doped perovskite nanocrystals (NCs). The NCs in the resulting composite have an average diameter of 8 nm and a photoluminescence quantum yield (PLQY) exceeding 30%. In addition, the optical properties of the $Cs(Pb_x/Mn_{1-x})Cl_3$@MSNs composite can be tuned by varying the Mn^{2+} doping level. The resulting composites presented a significantly improved resistance to UV light, temperature, and moisture compared to the bare $Cs(Pb_{0.72}/Mn_{0.28})Cl_3$. Finally, we fabricated down-converting white light emitting diodes (WLEDs) by using $Cs(Pb_x/Mn_{1-x})Cl_3$@MSNs composite as the orange-emitting phosphor deposited onto UV emitting chips, demonstrating their promising applications in solid-state lighting. This work provides a valuable approach to fabricate stable orange luminophores as replacements for traditional emitters in LED devices.

KEYWORDS: mesoporous silica nanospheres, Mn^{2+}-doped $CsPbCl_3$ nanocrystals, photostability, orange emitter, WLED.

Introduction

Recently, colloidal caesium lead halide-based perovskite nanocrystals ($CsPbX_3$ NCs, X = Cl, Br or I) have been shown to possess exceptional optical properties, including bright photoluminescence (PL) with quantum yields ≥90%, a wide gamut of colours, narrow full width at half maximum (FWHM), and bandgaps adjustable by tuning the halide composition and the crystal morphology.[1-5] Overall, these remarkable features make perovskite nanocrystals (NCs) excellent candidates as the next generation of illumination sources for a wide range of optoelectronic applications, including light-emitting diodes (LEDs), anti-counterfeit inks, lasers, photodetectors, and display backlights.[5-10]

However, their instability in ambient environment, heat, and UV light, as well as the facile anion exchange reaction and phase transformation, limits their practical applications. These issues arise from the low formation energy and the considerable ionic character of the perovskite NCs.[1, 5, 11-15] Progress to correct the inherent vulnerability of perovskite NCs has already been demonstrated. Embedding $CsPbX_3$ NCs into inorganic (SiO_2, metal-organic frameworks, or zeolite-Y)[16-20] or polymer matrices (polystyrene, polymethyl methacrylate, block copolymer micelles, or polyvinylidene fluoride),[21-25] can preserve the bright emission while improving stability. Regulating the surface capping by introducing long-chain,[26-27] polydentate chelating,[28] branched [29] or sterically-hindered surfactants[30] as ligands to create surface passivation layers is also effective. Beyond those, doping with other cations has been shown to stabilize the material, with Mn^{2+} identified as an effective option.[31-34] Mn^{2+} and Pb^{2+} possess the same valence state and similar ionic radii with a higher bond dissociation energy (Mn-Cl relative to Pb-Cl), which allows for the partial replacement of Pb in $CsPbCl_3$ with Mn.[31,33, 35]

While such efforts can enhance the stability of the NCs,[17-18, 22-23, 28] the ability to obtain stable nano-scale perovskites remains a challenge.[21, 36-37] Some of the attempts resulted in materials only suitable to prepare bulk luminescent materials[18, 22-23] and offered a limited improvement in resistance to water and UV light.[21, 36] Therefore, in order to obtain high stability without significant loss of the unique electrical and optical properties in ambient air and under UV light, it is essential to develop a facile and efficient synthetic method to produce monodispersed and stable nanocrystal composites.

To date, a wide variety of porous materials have been used to host inorganic crystals and improve their stability.[16, 38-41] Mesoporous silica nanospheres (MSNs) are a fascinating class of porous materials and have been extensively studied because of their tuneable pore sizes, large internal pore volume and extensive pore connectivity, conferring them with a high specific area, excellent stability, easier surface functionalization, and non-toxicity.[42-44] These outstanding features make MSNs a promising platform for confined growth of nanoparticles within the pores.[43-44]

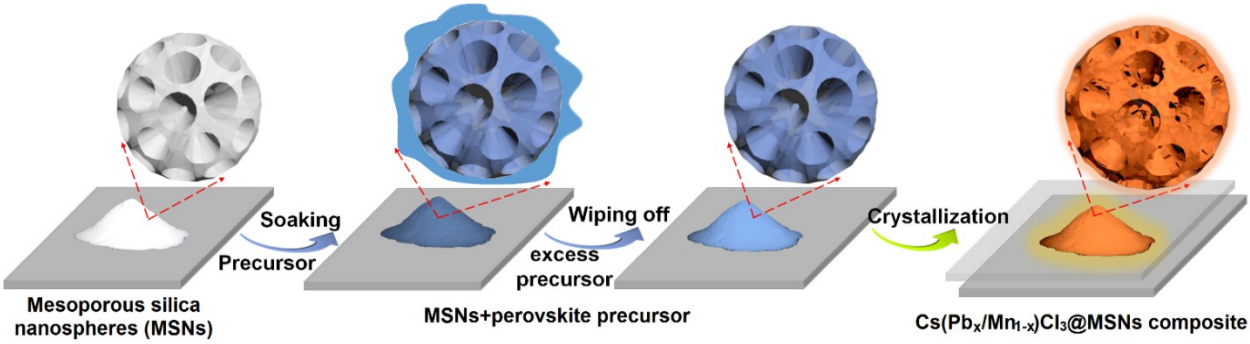

Scheme 1. Schematic illustration of the *in-situ* formation and crystallization strategy of the $Cs(Pb_x/Mn_{1-x})Cl_3$@MSNs composites.

In this study, we present a synthetic strategy to grow $Cs(Pb_x/Mn_{1-x})Cl_3$ (x denotes the Pb composition out of the total Pb/Mn) NCs within the pores of MSNs (Scheme 1). This facile and

effective strategy can not only yield large scale of ligand-free NCs with controllable size and diversified component, but also confine and separate spatially for inhibiting NCs sintering by dendritic templates. Mn^{2+} has good compatibility with the cations in $CsPbCl_3$ and provides a new exciton transition pathway offering control of emission color (Table S1).[31-33] The Mn^{2+}-doped perovskite in porous silica has improved resistance to elevated temperatures and UV irradiation, and serves as a good fluorophore in down converting white light-emitting diodes (WLED). Additionally, Mn^{2+}-doping perovskite NCs reduces the toxic Pb^{2+} used, a concern in industrial applications.[32,48 45] The optical properties of the $Cs(Pb_x/Mn_{1-x})Cl_3$@MSNs composite were varied by tuning the stoichiometry of the Mn^{2+}-doping level. The photo and thermal stability of the as-prepared $Cs(Pb_x/Mn_{1-x})Cl_3$@MSNs composites were evaluated by comparing the relative photoluminescence quantum yields (PLQY) before and after exposure. Finally, the use of the composites as organic fluorophores in WLED was explored, demonstrating the materials' value as a stable luminophore in optoelectronic devices.

EXPERIMENTAL SECTION

Synthesis: The mesoporous silica nanoparticles (MSNs) were prepared following a modified procedure via a template-assisted *sol-gel* technique.[42] We used cetyl-trimethylammonium tosylate (CTAT*os*) as the templating surfactant and triethanolamine ($TEAH_3$) as the mineralizing agent (see Supplemental Information).

Template-assisted synthesis of Mn^{2+} doped lead halide perovskite nanocrystals in MSNs is conducted following a modified procedure, [40] as outlined in Scheme 1. A typical synthesis procedure is described as the following: The MSNs were dried at 150° C for 12 h under vacuum

before using. Then, 2.0 mg of mesoporous silica nanoparticles were impregnated with 10 μL 0.3 M solution of Cs_2CO_3, $PbCl_2$ and $MnCl_2$ (molar ratio of Cs_2CO_3:$PbCl_2$:$MnCl_2$ is 0.5:1:5 or 0.5:1:10) in dimethyl sulfoxide (DMSO). After impregnation, the excess solution was removed by damping with filter paper. The powder was sandwiched between two glass slides and heated up to 120°C in a vacuum oven for 120 minutes. Afterwards, the powder was allowed to cool to 50 °C under vacuum and then to room temperature in vacuum oven. Finally, the powder was dispersed and washed with *n*-hexane and isopropanol three times and centrifuged, after which the powder was collected for further characterization. Finally, the resulting composite was dried in a vacuum oven overnight before being used. The composites of $CsPbBr_3$@MSNs and $CsPb(Br/Cl)_3$@MSNs were prepared following the same procedure above.

Stability Tests: To evaluate the thermal-stability and photo-stability, the powders of $Cs(Pb_x/Mn_{1-x})Cl_3$@MSNs composite were stored in a flask upon increased temperature and subjected to UV light irradiation (365 nm, 0.5 $W \cdot cm^{-2}$), and PL intensity was subsequently measured over different period of times. Besides, the powder of $Cs(Pb_x/Mn_{1-x})Cl_3$@MSNs composites was exposed atmospheric moisture over times. The aged samples were then subjected to further characterization.

White LED device fabrication: For white LED device fabrication, UV (365 nm) LED chips was used to excite the blue $CsPb(Cl/Br)_3$@MSNs (458 nm) and orange $Cs(Pb_x/Mn_{1-x})Cl_3$@MSNs (588 nm) composites. Firstly, the $CsPb(Cl/Br)_3$@MSNs composite (0-0.3 g) was dispersed in silicon resin (3 g) after vigorous stirring, and the obtained mixture was directly coated onto UV LED chips and thermally cured at 40 °C for 30 min and 120 °C for 60 min, gradually. Then, $Cs(Pb_x/Mn_{1-x})Cl_3$@MSNs layer was prepared similarly as above, which would be stowage onto

the upper surface of blue-based LED devices by mixing with silicon resin, followed by two-stage thermal curing, to give the fabricated WLED devices.

Characterization Methods: Ultraviolet and visible absorption (UV-vis) spectra of composites were collected using a Cary 5000 UV-Vis-NIR spectrophotometer. Fluorescence spectra fluorescent lifetime and absolute photo-luminescent quantum yields (PLQYs) were collected using an integrated sphere on an Edinburgh Instruments FLS920 spectrophotometer. The Powder X-ray diffraction (PXRD) patterns were acquired using a Bruker AXS D8 Discover X-Ray Diffractometer at a wavelength of Cu K (1.79 Å). X-Ray photoelectron spectroscopy (XPS) measurement of elemental composition was conducted on the composite powder by an AXIS ULTRA (England, KRATOS ANALYTICAL Ltd) using an Al mono Kα X-ray source (1486.6 eV) operated at 150 W. SEM images were acquired on a JEOL 7800F Field Emission Scanning Electron Microscope. TEM, high-resolution TEM (HR-TEM) and elemental composition were acquired on a FEI G_2F_{30} electron microscope operated at 200 kV with a Gatan SC 200 CCD camera equipped with an EDS. The Brunauer-Emmet-Teller (BET) and Barrett-Joyner-Halenda (BJH) methods were characterized for pore size distributions and specific surface areas by an ASAP 2010 Micrometrics sorptometer (USA).

Results and discussion

The overall synthetic strategy for the $Cs(Pb_x/Mn_{1-x})Cl_3$@MSNs composites is shown in Scheme 1. Mesoporous silica nanoparticles were soaked with precursor solution of Cs_2CO_3, $PbCl_2$, and $MnCl_2$ in DMSO with the Pb concentration kept at 0.3 M.[40] Attempts to prepare the composites by stacking the saturated MSNs onto glass for crystallization at 120 °C produced only weak

fluorescence, possibly due to the uneven heating of the surface (Figure S1). To correct this, the saturated powder was sandwiched between two glass slides to even heating at 120 °C. The composites turned from white to yellow upon solvent volatilization. Finally, the yellow powder was then collected after 120 minutes by cooling under vacuum. Finding the optimum crystallization temperature was crucial to the success of the process. Elevated temperatures cause carbonization of the organic solvent and promote uneven growth of the NCs (Figure S1). At lower temperatures, the NCs do not form (Figure S1). The composites made from different Pb/Mn feed ratios led to varying Pb/Mn composition in the formula $Cs(Pb_x/Mn_{1-x})Cl_3$. For example, from the feed Pb/Mn ratios of 1:5 and 1:10, x is determined to be 0.84 and 0.66, respectively (see later discussions).

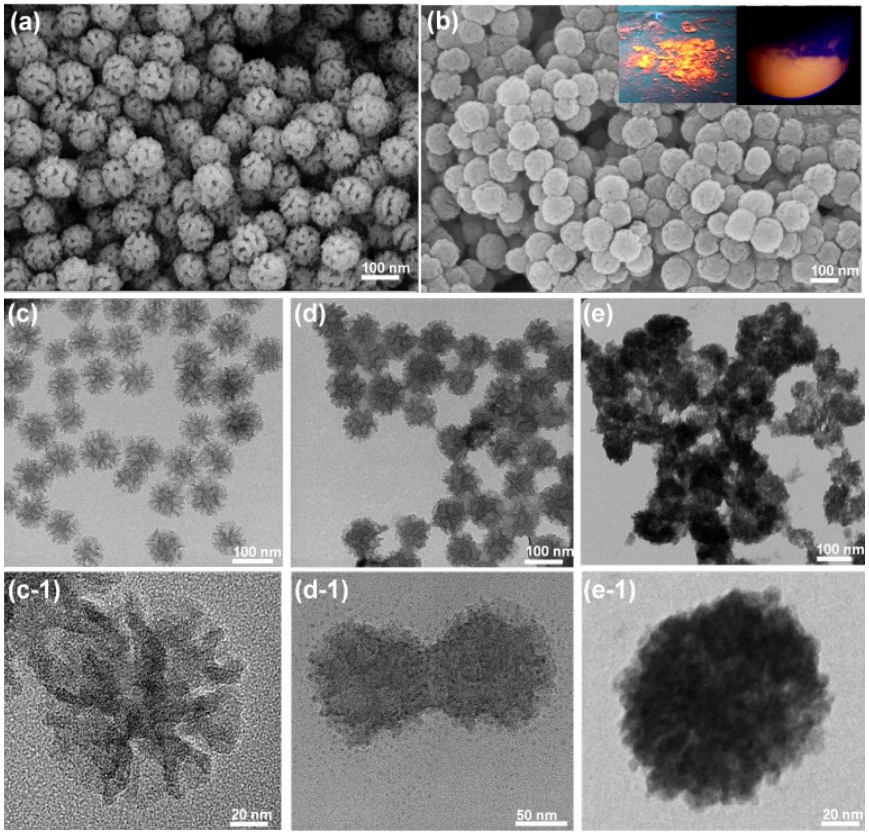

Figure 1. Morphologies of the $Cs(Pb_{0.66}/Mn_{0.34})Cl_3$@MSNs composites. SEM images of pristine MSNs (a) and $Cs(Pb_{0.66}/Mn_{0.34})Cl_3$@MSNs composites (b). Insets in (b) are the digital images of

the *as*-synthesized composite under UV light (365 nm). Low and high magnification TEM images of the MSNs (c and c-1), MSNs saturated with precursors (d and d-1), and $Cs(Pb_{0.66}/Mn_{0.34})Cl_3$@MSNs composites (e and e-1).

Transmission (TEM) and scanning electron microscopy (SEM) were used to investigate the morphology of the $Cs(Pb_{0.66}/Mn_{0.34})Cl_3$@MSNs composites (Figure 1). The MSNs present a uniform spherical morphology with typical center-radial dendritic structures and an average diameter of approximately 105 nm (Figure 1a, c and S2). We measured the pore mouth diameter to be in the 10-14 nm range, which closely matches the average 13.3 nm pore size of the MSNs calculated from the Brunauer-Emmett-Teller (BET) isotherms (Figure 2c). The MSNs present a large pore volume (0.966 cc/g) and surface area (337.82 m^2 g^{-1}) calculated from BET method. Per design, the large surface area, internal pore volumes and high pore connectivity favour incorporation of $Cs(Pb_x/Mn_{1-x})Cl_3$ NCs as a guest.[40, 42, 44, 46-47]

To obtain more insight into the reaction process, we examined the morphology of the mesoporous silica particles saturated with precursors, shown in Figure 1d. Uniform particles with filled the dendritic pores were observed. Compared with the pure MSNs, $Cs(Pb_{0.66}/Mn_{0.34})Cl_3$@MSNs composites have a denser surface, presumably because the NCs have occupied the pore space (Figure 1b and e). More detailed TEM characterization images taken at different locations (Figures S2 and S3) further proved that crystallized $Cs(Pb_{0.66}/Mn_{0.34})Cl_3$ was present inside the templated pore channels. In comparison, the free $Cs(Pb_x/Mn_{1-x})Cl_3$ NCs without MSNs displays irregular morphologies (nanocubes and sheet-like crystals), broader size distributions (25-200 nm) and much larger sizes (Figures S3).To further confirm the formation of $Cs(Pb_x/Mn_{1-x})Cl_3$@MSNs composites, we examined with high resolution (HR) TEM (Figure 2a). HR-TEM observation reveals that the NCs have visible crystal lattices of the tetragonal

$CsPbCl_3$.[32, 33, 45] The embedded NCs are distributed uniformly inside the mesoporous SiO_2 particles with an average diameter of 8 nm (Figures 2a and S3). Notably, no excessively large particles were observed, which implies the inclusion of the smaller size NCs rather than exclusion of larger particles. SEM-EDS elemental composition mappings for Si, Cs, Pb, Mn, and Cl elements from composites are presented in Figure 2b. As expected, all the related elements can be detected uniformly.

There is a large decrease of MSNs pore volume (0.966 to 0.238 cc/g) and surface area (337.82 to 38.70 m^2 g^{-1}) after growth of the NCs. The corresponding signature for the average pore diameter has disappeared (Figure 2c), further demonstrating the successful encapsulation of the NCs inside the MSNs.

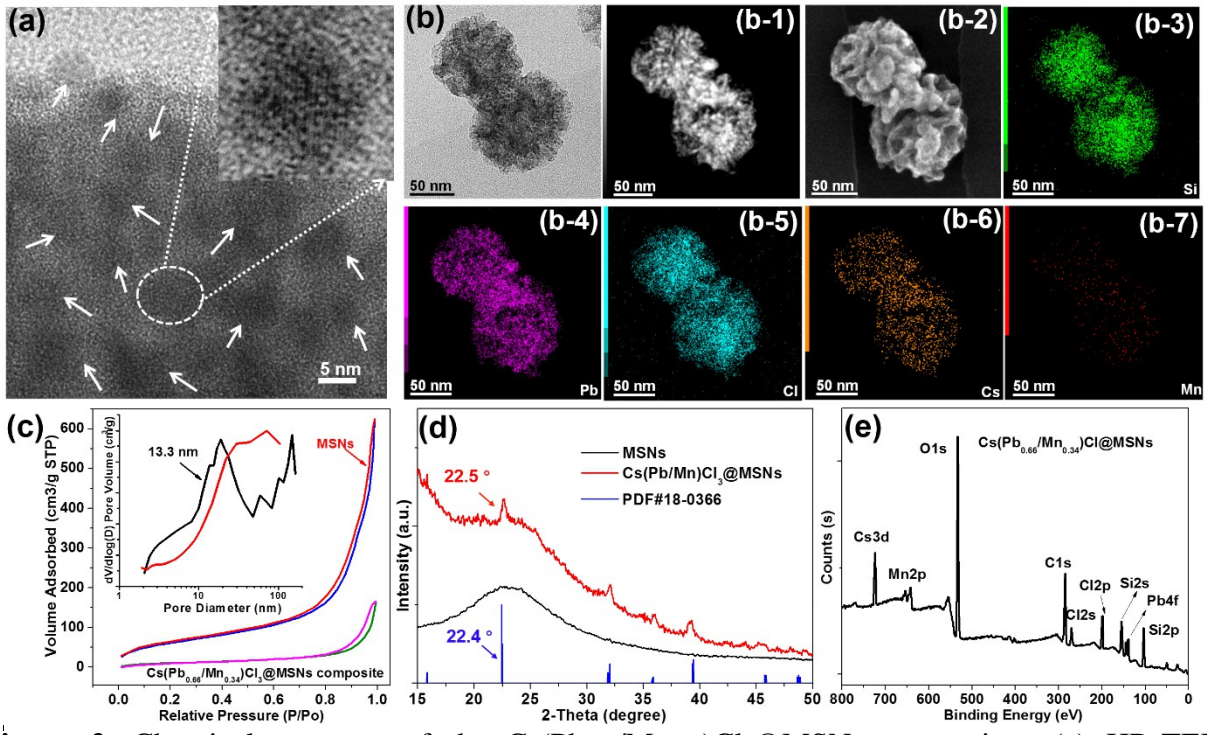

Figure 2. Chemical structure of the $Cs(Pb_{0.66}/Mn_{0.34})Cl_3$@MSNs composites. (a) HR-TEM images of the typical morphology of the $Cs(Pb_{0.66}/Mn_{0.34})Cl_3$@MSNs composites. White arrows mark the embedded perovskite nanocrystals. (b) TEM, STEM and TEM elemental mapping profiles for the Si, Pb, Cl, Cs, and Mn elements. (c) N_2 adsorption/desorption isotherms and the

corresponding pore size distribution (inset) for the MSNs and the $Cs(Pb_{0.66}/Mn_{0.34})Cl_3$@MSNs composites. (d) Experimental powder X-ray diffraction (PXRD) patterns and comparison to the standard tetragonal crystal structure of $CsPbCl_3$ (PDF#18-0366). (e) High-resolution X-ray photoelectron spectra (XPS) analysis with a survey scan..

Powder X-ray diffraction patterns (XRD) were measured to identify the crystal structure of the resulting $Cs(Pb_{0.66}/Mn_{0.34})Cl_3$@MSNs composites (Figure 2d). The $Cs(Pb_{0.66}/Mn_{0.34})Cl_3$@MSNs powder exhibits the tetragonal crystalline structure of bulk $CsPbCl_3$ (JCPDF #18-0366) with a 0.1° shift toward higher angles when Mn replaces Pb (22.4° to 22.5°, Figure 2d).[48-49] The broad peak around 22° is attributed to amorphous SiO_2.[40] XPS elemental composition analysis also confirmed that the *as*-obtained Mn^{2+}-doped perovskite powder contained all the elements (Cs3d5, C1s, Si2s, Pb4f, Mn2p and Cl2s) expected from the $Cs(Pb_x/Mn_{1-x})Cl_3$ and MSNs (Figure 2e and S4). The quantification elemental ratio for Cs:Pb/Mn:Cl measured by XPS was about 0.92:0.66/0.34:3.20, which matches well with the ratio in the Mn-doped perovskite $Cs(Pb_{0.66}/Mn_{0.34})Cl_3$. All the collected results confirm the NCs were successfully embedded in the MSNs matrices as presented in the schematic illustrations (Scheme 1).

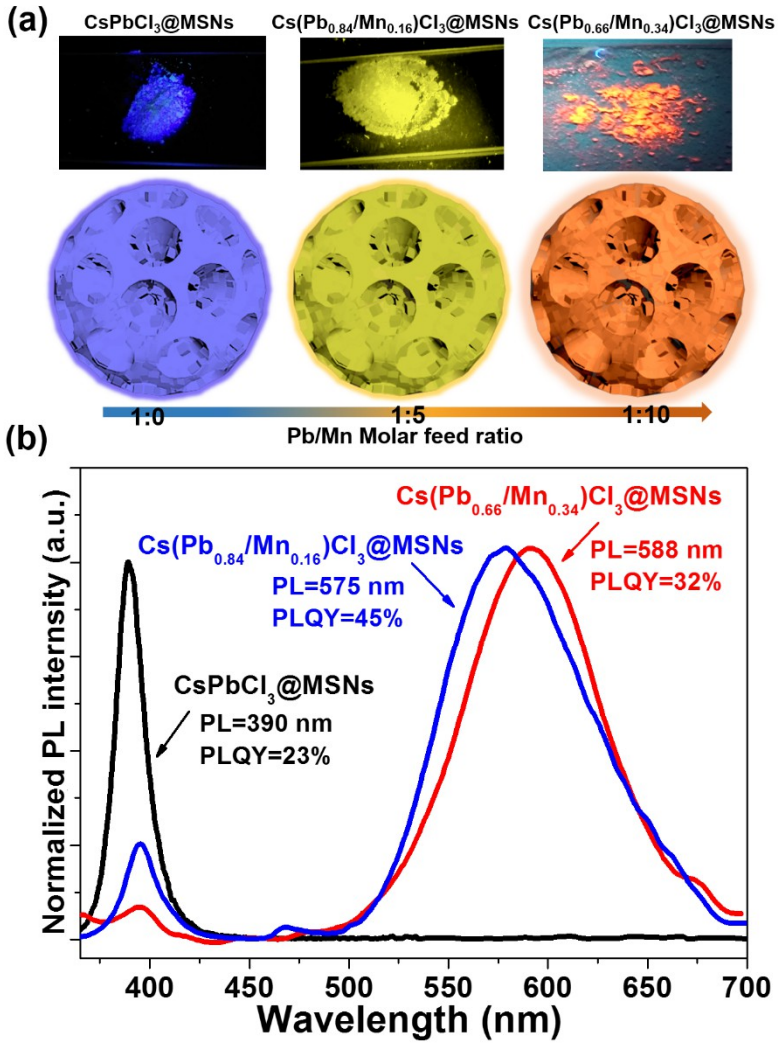

Figure 3. Optical properties of $Cs(Pb_x/Mn_{1-x})Cl_3$@MSNs composites. (a) Optical photographs and schematic illustrations of $CsPbCl_3$@MSNs, $Cs(Pb_{0.84}/Mn_{0.16})Cl_3$@MSNs and $Cs(Pb_{0.66}/Mn_{0.34})Cl_3$@MSNs powders with different Pb-to-Mn molar feed ratios under UV light; (b) Photoluminescence spectra of the $CsPbCl_3$@MSNs, $Cs(Pb_{0.84}/Mn_{0.16})Cl_3$@MSNs and $Cs(Pb_{0.66}/Mn_{0.34})Cl_3$@MSNs composites, listing the corresponding PL emission maxima and PLQY.

In analogy with the modulation of perovskite NCs band gaps through control of anion composition,[1-2, 50, 51] the band gap of Mn^{2+} doped perovskite NCs can be easily adjusted by varying the Pb/Mn ratio (Table S1).[48, 52] Using the same synthetic route, we can grow several $Cs(Pb_x/Mn_{1-x})Cl_3$@MSNs composites with various Pb/Mn ratios. When decreasing the Pb to Mn

molar feed ratio from 1:0 to 1:5, then 1:10, the measured composition changed from $CsPbCl_3$@MSNs, $Cs(Pb_{0.84}/Mn_{0.16})Cl_3$@MSNs to $Cs(Pb_{0.66}/Mn_{0.34})Cl_3$@MSNs (Figure 3a). The corresponding photoluminescence (PL) spectra of the selected $Cs(Pb_x/Mn_{1-x})Cl_3$@MSNs composites are shown in Figure 3b. The PL emission peak maximum of the $Cs(Pb_x/Mn_{1-x})Cl_3$@MSNs shifted towards higher wavelengths with increasing Mn content.[45, 48] Specifically, the emission onset occurred at 390 nm, 575 nm and 588 nm for $CsPbCl_3$@MSNs, $Cs(Pb_{0.84}/Mn_{0.16})Cl_3$@MSNs and $Cs(Pb_{0.66}/Mn_{0.34})Cl_3$@MSNs composites, respectively (Figure 3b), which we attributed to the enhancement of exciton-to-Mn^{2+} energy transfer, similar to that reported for free Mn-based perovskite NCs (Table S1).[45, 48, 52] The absorption spectra however remains identical, with an absorption peak maximum at 382 nm (Figure S5a) when the Pb-to-Mn molar feed ratio changes. Notably, the PL excitation spectrum (collected by monitoring the PL centered at 575 and 588 nm) closely follows the absorption spectrum (Figure S5b), further implying that the broad-band emission of Mn^{2+} is sensitized by the $CsPbCl_3$ NC host, consistent with reports for free Mn-based perovskite NCs.[32, 48] Besides, different from the multiexponential decay (t_1=0.86 ns and t_2=9.73 ns) of the 390 nm emission, Mn^{2+} emission lifetime at 588 nm shows a single exponential decay with a longer lifetime of 1.02 ms, ascribing to the Mn^{2+} emission with the energy transferred from excitons of $CsPbCl_3$ NCs. All the results suggest a nearly homogeneous environment of Mn dopants inside the $CsPbCl_3$ host, consistent with the previous report of the Mn^{2+}-doped perovskite NCs.[32, 33, 45, 49] Additionally, the PLQY value was near 45% and 32% for $Cs(Pb_{0.84}/Mn_{0.16})Cl_3$@MSNs and $Cs(Pb_{0.66}/Mn_{0.34})Cl_3$@MSNs, respectively, much higher than that for $CsPbCl_3$@MSNs (23%) and $Cs(Pb_{0.72}/Mn_{0.28})Cl_3$ NCs (12%) obtained under the same conditions (Figure S6). This is because the pore of the MSNs can confine the growth of perovskite NCs, yielding with smaller size than the $Cs(Pb_{0.72}/Mn_{0.28})Cl_3$

NCs.[39, 41] Composites with higher Mn content present a significant reduction of the PLQY, presumably excessive Mn substitution destroys the crystallinity of the $CsPbCl_3$ NCs, in agreement with previous reports.[32, 45, 48] Furthermore, the mesoporous matrix is also suitable for growing $CsPbBr_3$@MSNs composites, leading to PL emission at 526 nm and a 53% PLQY.

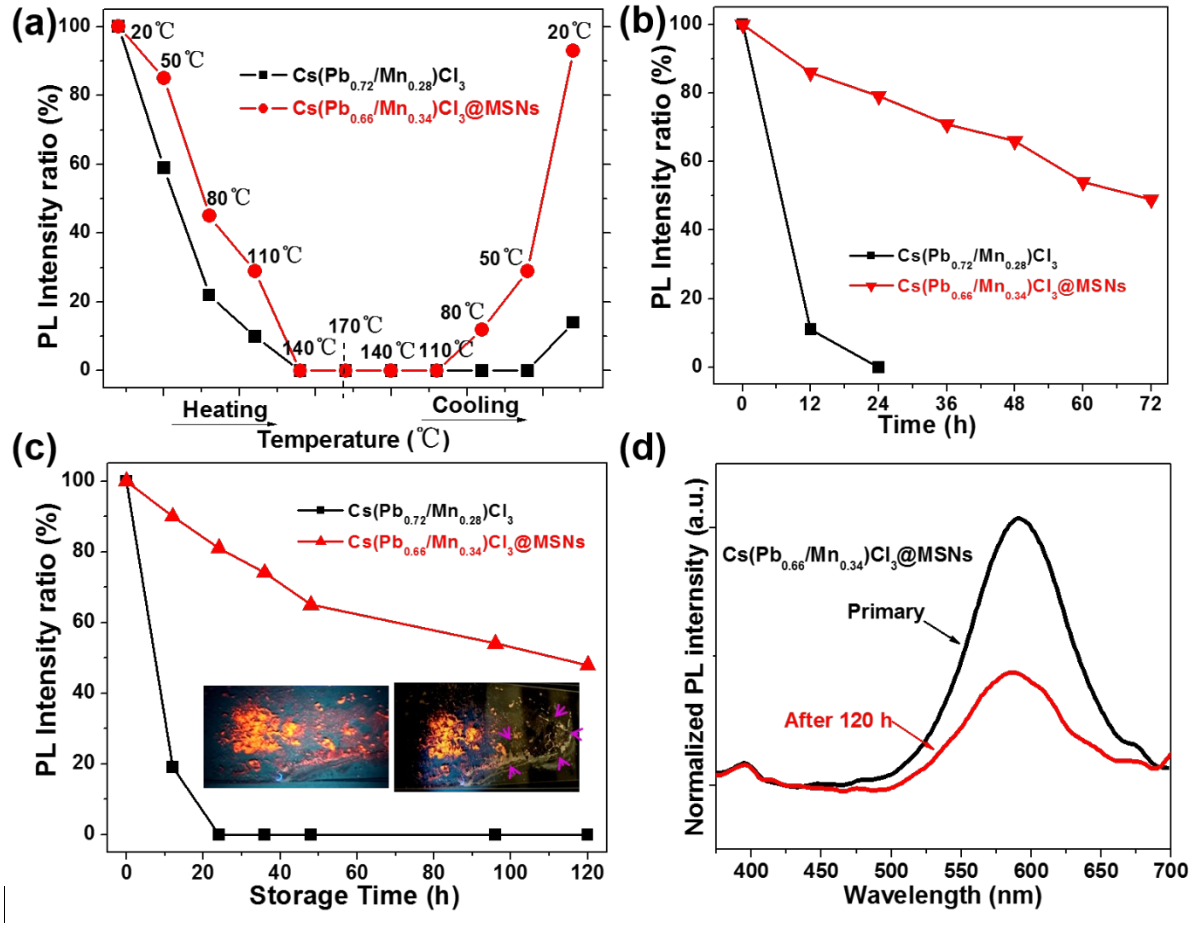

Figure 4. Improved stability of the $Cs(Pb_x/Mn_{1-x})Cl_3$@MSNs composites. (a) Relative PLQY as a function of temperature. (b) Relative PLQY plots as a function of UV irradiation time. (c) Relative PLQY plots over time of $Cs(Pb_{0.72}/Mn_{0.28})Cl_3$ and $Cs(Pb_{0.66}/Mn_{0.34})Cl_3$@MSNs after exposure to atmospheric moisture. Insets in (c) are the photographs of $Cs(Pb_{0.66}/Mn_{0.34})Cl_3$@MSNs after exposition to atmospheric moisture for 120 h. (d) Photoluminescence spectra of $Cs(Pb_{0.66}/Mn_{0.34})Cl_3$@MSNs composites before and after exposure at atmospheric moisture for 120 h.

During the growth process, the spatial isolation of $Cs(Pb_x/Mn_{1-x})Cl_3$ NCs in the MSN cavities effectively prevented close contact and particle fusion.[42, 44] The shielding effect in the thus formed suprastructures is also likely to yield improved stability towards UV light, temperature, and atmospheric moisture. We measured the stability of $Cs(Pb_{0.66}/Mn_{0.34})Cl_3$@MSNs composites by comparing them with bare $Cs(Pb_{0.72}/Mn_{0.28})Cl_3$ NCs.

The thermal stability of the $Cs(Pb_{0.66}/Mn_{0.34})Cl_3$@MSNs composite was tested by heating to 170 °C and cooling to room temperature (20 °C) (Figure 4a). The photoluminescence of $Cs(Pb_{0.66}/Mn_{0.34})Cl_3$@MSNs composite (588 nm) decreased with increasing temperature, and completely quenched at 170 °C, indicating a typical thermal quenching behaviour (Figure 4a). The photoluminescence intensity of $Cs(Pb_{0.66}/Mn_{0.34})Cl_3$@MSNs composite then increased as temperature was decreased from 170 °C to 20 °C. The process was mostly reversible, with a small loss of 3.6% after cycling. The bare $Cs(Pb_{0.72}/Mn_{0.28})Cl_3$ NCs presented a similar decrease in PL with increasing temperature, but only recovered ca. 20% of their initial value on cooling. The results of the temperature-dependent PL properties and thermally-induced switching of $Cs(Pb_{0.66}/Mn_{0.34})Cl_3$@MSNs composites would be valuable in long-term LED operation.

To evaluate the photostability of the prepared $Cs(Pb_{0.66}/Mn_{0.34})Cl_3$@MSNs composite, we measured the relative PL intensity at different times under continuous UV irradiation (365 nm) (Figure 4b). Because of the absence of a passivation matrix, the relative PL intensity of the bare $Cs(Pb_{0.72}/Mn_{0.28})Cl_3$ NCs decreased dramatically, and was fully quenched within 24 h, accompanied by a visible shift in colour from green to yellow (Figure 4b). For the $Cs(Pb_{0.66}/Mn_{0.34})Cl_3$@MSNs composite, however, where the MSNs serve as a protective matrix, the relative PL intensity was still 80% of the initial value after 24 h. Even after 72 h, more than

50% of the initial intensity was preserved (Figure 4b). Conceptually, the NCs provide spatial isolation in the pores, inhibiting particle fusion generally promoted by light or heat. Similar results were reported when isolating NCs inside polymer or inorganic matrix.[17, 22-24]

To measure stability to moisture, we performed comparative studies of bare $Cs(Pb_{0.72}/Mn_{0.28})Cl_3$ and $Cs(Pb_{0.66}/Mn_{0.34})Cl_3$@MSNs. Materials were exposed to atmospheric moisture (relative humidity of approximately 40%) for 24 h, as shown in Figure 4c. The relative PL was recorded at different times. When exposed to atmospheric moisture (RH=40%), the PLQYs of bare $Cs(Pb_{0.72}/Mn_{0.28})Cl_3$ decreased quickly to less than 20% of the initial value after 12 h of exposure. $Cs(Pb_{0.66}/Mn_{0.34})Cl_3$@MSNs retained a 90% of its initial intensity after 12 h. Photographs inset in Figure 4c, Figure S7, and Figure 4d further confirm that the $Cs(Pb_{0.66}Mn_{0.34})Cl_3$@MSNs films remain bright even after being exposed to atmospheric moisture for 120 h. Taken together, our results demonstrate that the $Cs(Pb_{0.66}/Mn_{0.34})Cl_3$@MSNs composites effectively shield the nanocrystals from environmental agents including UV light, temperature and moisture, which makes them good candidates for use in optoelectronic devices.[39-41, 44]

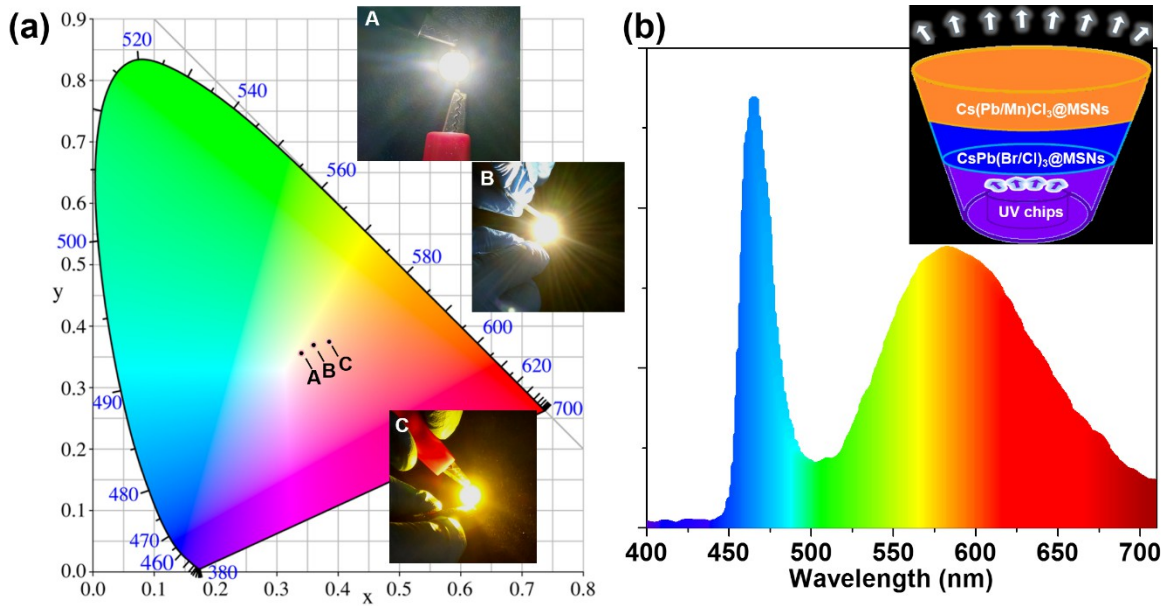

Figure 5. Performance of the WLED. (a) CIE color coordinates of the fabricated WLED devices with various contents of $Cs(Pb_{0.66}/Mn_{0.34})Cl_3$@MSNs composites. The insets are photographs of the corresponding devices working under an applied current of 20 mA. (b) Emission spectra of the WLED. The inset shows the schematic structure of the WLED, composed of UV (365 nm) chips, $CsPb(Br/Cl)_3$@MSNs and $Cs(Pb_{0.66}/Mn_{0.34})Cl_3$@MSNs composites mixed with silicone resin.

$Cs(Pb_x/Mn_{1-x})Cl_3$@MSNs composites demonstrated excellent optical properties and good stability as an orange fluorophore. In a proof of concept demonstration, we used the composites in a down-converting white light emitting device (WLED). The typical WLED device structure is shown in Figure 5, where the Mn^{2+}-doped $Cs(Pb_{0.66}/Mn_{0.34})Cl_3$@MSNs composite and $CsPb(Br/Cl)_3$@MSNs (Figure S6g) was mixed with silicone resin and deposited on a UV-emitting chip (365 nm) in LED packaging. Similar to the PL spectrum, the photoluminescence (PL) spectrum of the prepared WLED device presents a broad orange emission peak centered at 589 nm and narrow blue emission peak centered at 460 nm when excited by the 365 nm GaN UV LED operating at 20 mA constant current (Figure 5). By changing the amounts of the $Cs(Pb_{0.66}/Mn_{0.34})Cl_3$@MSN composite, orange, yellow, and white LEDs can be obtained (inset in

Figure 5a). Saturated and bright white emission can be realized with optimized ratios. A CIE colour coordinate (0.342, 0.356) was obtained, very close to standard white emission (0.33, 0.33).

The fabricated WLED exhibits a luminous efficacy (LE) of 62.5 lm/W. The color rendering index (CRI) and the correlated color temperatures (CCTs) are 82 and 5766 K, respectively, which enables the potential use of the composite in optoelectronic devices. The composite exhibits a gradual increase in emission intensity as the current increases, sustaining constant emission even when the GaN source was operated at 200 mA (Figure S9a). The normalized spectra present a slight loss at 589 nm emission (Figure S9b), indicating the Mn^{2+}-doped $Cs(Pb_{0.66}/Mn_{0.34})Cl_3$@MSN degrade slightly under strong current, superior than reported free perovskite and zeolite encapsulated perovskite.[16] Besides, the PL intensity of the fabricated WLED can retain at least 90% or 65% of the initial intensity after exposure to atmospheric moisture for 10 days or continuous working for 30 min, respectively, shown in Figure S9c. This strong fluorescence and improved stability confers great potential to the $Cs(Pb_x/Mn_{1-x})Cl_3$@MSNs composite as a fluorophore for the fabrication of wide-colour gamut light sources and displays.

Conclusions

In summary, we report a facile and effective synthesis to create highly luminescent and stable $Cs(Pb_x/Mn_{1-x})Cl_3$@MSNs composites by growing Mn^{2+} doped $CsPbCl_3$ nanocrystals embedded in mesoporous silica nanospheres (MSNs). The MSNs were prepared via a templated *sol-gel* technique, yielding monodispersed center-radial dendritic porous particles of 105 nm and pore sizes of 13.3 nm. The well-defined $Cs(Pb_x/Mn_{1-x})Cl_3$@MSNs composites were subsequently

fabricated by employing the MSNs as the matrix to grow $Cs(Pb_{0.66}/Mn_{0.34})Cl_3$ NCs (approximately 8 nm). The resulting composites exhibit a high photoluminescence quantum yield (PLQY) exceeding 32%, a tuneable emission wavelength governed by the Pb-to-Mn ratio, and enhanced photostability and thermostability. The prepared $Cs(Pb_{0.66}/Mn_{0.34})Cl_3$@MSNs composite can be used in a WLED as the orange emitter, an example of their promising future in solid-state lighting. We believe our results will pave the way for extensive research on Mn-doped perovskite composites with exceptional optoelectronic properties.

Supporting Information Available

Experimental details of MSNs and $Cs(Pb_x/Mn_{1-x})Cl_3$@MSNs composite; The summary of the morphology, chemical structures and optical properties of the MSNs and composites with Pb-to-Mn ratio and $CsPbBr_3$ by TEM, SEM and XPS. This material is available free of charge via the Internet at http://pubs.acs.org.

AUTHOR INFORMATION

Corresponding Author

*Email: panaizhao2017032@xjtu.edu.cn.

*Email: heling@mail.xjtu.edu.cn.

*Email: yliu@lbl.gov.

Author Contributions

All authors have given approval to the final version of the manuscript.

Notes

The authors declare no competing financial interest.

ACKNOWLEDGMENT

This work was supported by the National Natural Science Foundation of China (NSFC Grants 51802254, 51873173), the China Postdoctoral Science Foundation Funded Project (2017M623149), the Fundamental Research Funds for the Central Universities (xjj2018053) and Shaanxi province Youth Foundation (2018JQ5011). This work was also supported by the U.S. Department of Energy, Office of Science, Office of Basic Energy Sciences, Materials Sciences and Engineering Division, under Contract No. DE-AC02-05-CH11231 within the Inorganic/Organic Nanocomposites Program (KC3104) (MJ and YL). Work at the Molecular Foundry was supported by the Office of Science, Office of Basic Energy Sciences, of the U.S. Department of Energy under Contract No. DE-AC02-05CH11231. The authors wish to express their gratitude to the MOE Key Laboratory for Nonequilibrium Condensed Matter and Quantum Engineering of Xi'an Jiaotong University. The authors also thank Jiao Li at Instrument Analysis Center of Xi'an Jiaotong University for their assistance with TEM analysis.

REFERENCES

(1) Protesescu, L.; Yakunin, S.; Bodnarchuk, M. I.; Krieg, F.; Caputo, R.; Hendon, C. H.; Yang, R. X.; Walsh, A.; Kovalenko, M. V. Nanocrystals of Cesium Lead Halide Perovskites ($CsPbX_3$, X = Cl, Br, and I): Novel Optoelectronic Materials Showing Bright Emission with Wide Color Gamut. *Nano Lett.* **2015,** *15*, 3692-3696.
(2) Nedelcu, G.; Protesescu, L.; Yakunin, S.; Bodnarchuk, M. I.; Grotevent, M. J.; Kovalenko, M. V. Fast Anion-Exchange in Highly Luminescent Nanocrystals of Cesium Lead Halide Perovskites ($CsPbX_3$, X= Cl, Br, I). *Nano Lett.* **2015,** *15*, 5635-5640.
(3) Bekenstein, Y.; Koscher, B. A.; Eaton, S. W.; Yang, P. D.; Alivisatos, A. P. Highly Luminescent Colloidal Nanoplates of Perovskite Cesium Lead Halide and Their Oriented Assemblies. *J. Am. Chem. Soc.* **2015,** *137*, 16008-16011.
(4) Swarnkar, A.; Chulliyil, R.; Ravi, V. K.; Irfanullah, M.; Chowdhury, A.; Nag, A. Colloidal $CsPbBr_3$ Perovskite Nanocrystals: Luminescence beyond Traditional Quantum Dots. *Angew. Chem. Int. Edit.* **2015,** *54*, 15424-15428.
(5) Kovalenko, M. V.; Protesescu, L.; Bodnarchuk, M. I. Properties and Potential Optoelectronic Applications of Lead Halide Perovskite Nanocrystals. *Science* **2017,** *358*, 745-750.
(6) Yakunin, S.; Protesescu, L.; Krieg, F.; Bodnarchuk, M. I.; Nedelcu, G.; Humer, M.; De Luca, G.; Fiebig, M.; Heiss, W.; Kovalenko, M. V. Low-threshold Amplified Spontaneous Emission and Lasing from Colloidal Nanocrystals of Caesium Lead Halide Perovskites. *Nat. Commun.* **2015,** *6,8056-8063*.
(7) Veldhuis, S. A.; Boix, P. P.; Yantara, N.; Li, M. J.; Sum, T. C.; Mathews, N.; Mhaisalkar, S. G. Perovskite Materials for Light-Emitting Diodes and Lasers. *Adv. Mater.* **2016,** *28*, 6804-6834.
(8) Eaton, S. W.; Lai, M. L.; Gibson, N. A.; Wong, A. B.; Dou, L. T.; Ma, J.; Wang, L. W.; Leone, S. R.; Yang, P. D. Lasing in Robust Cesium Lead Halide Perovskite Nanowires. *P. Natl. Acad. Sci.* **2016,** *113*, 1993-1998.
(9) Chang, S.; Bai, Z. L.; Zhong, H. Z. In Situ Fabricated Perovskite Nanocrystals: A Revolution in Optical Materials. *Adv. Opt. Mater.* **2018,** *6*, 1800380-1800398.
(10) Tong, Y.; Bohn, B. J.; Bladt, E.; Wang, K.; Müller-Buschbaum, P.; Bals, S.; Urban, A. S.; Polavarapu, L.; Feldmann, J. From Precursor Powders to $CsPbX_3$ Perovskite Nanowires: One-Pot Synthesis, Growth Mechanism, and Oriented Self-Assembly. *Angew. Chem. Int. Edit.* **2017,** *56*, 13887-13892.
(11) Dang, Z. Y.; Shamsi, J.; Palazon, F.; Imran, M.; Akkerman, Q. A.; Park, S.; Bertoni, G.; Prato, M.; Brescia, R.; Manna, L. In Situ Transmission Electron Microscopy Study of Electron Beam-Induced Transformations in Colloidal Cesium Lead Halide Perovskite Nanocrystals. *ACS Nano* **2017,** *11*, 2124-2132.
(12) Wang, H. C.; Bao, Z.; Tsai, H. Y.; Tang, A. C.; Liu, R. S. Perovskite Quantum Dots and Their

Application in Light-Emitting Diodes. *Small* **2018,** *14*, 1702433-1702455.
(13) Kim, Y.; Yassitepe, E.; Voznyy, O.; Comin, R.; Walters, G.; Gong, X. W.; Kanjanaboos, P.; Nogueira, A. F.; Sargent, E. H. Efficient Luminescence from Perovskite Quantum Dot Solids. *ACS Appl. Mater. Inter.* **2015,** *7*, 25007-25013.
(14) Roo, J. D.; Ibáñez, M.; Geiregat, P.; Nedelcu, G.; Walravens, W.; Maes, J.; Martins, J. C.; Driessche, I. V.; Kovalenko, M. V.; Hens, Z. Highly Dynamic Ligand Binding and Light Absorption Coefficient of Cesium Lead Bromide Perovskite Nanocrystals, *ACS Nano*, 2016, 10, 2071-2081.
(15) Shamsi, J.; Rastogi, P.; Caligiuri, V.; Abdelhady, A. L.; Spirito, D.; Manna, L.; Krahne, R. Bright-Emitting Perovskite Films by Large-Scale Synthesis and Photoinduced Solid-State Transformation of $CsPbBr_3$ Nanoplatelets. *ACS Nano* **2017,** *11*, 10206-10213.
(16) Sun, J. Y.; Rabouw, F. T.; Yang, X. F.; Huang, X. Y.; Jing, X. P.; Ye, S.; Zhang, Q. Y. Facile Two-Step Synthesis of All-Inorganic Perovskite $CsPbX_3$ (X = Cl, Br, and I) Zeolite-Y Composite Phosphors for Potential Backlight Display Application. *Adv. Funct. Mater.* **2017,** *27*, 1704371-1704378.
(17) Zhong, Q. X.; Cao, M. H.; Hu, H. C.; Yang, D.; Chen, M.; Li, P. L.; Wu, L. Z.; Zhang, Q. One-Pot Synthesis of Highly Stable $CsPbBr_3@SiO_2$ Core-Shell Nanoparticles. *ACS Nano* **2018,** *12*, 8579-8587.
(18) Loiudice, A.; Saris, S.; Oveisi, E.; Alexander, D. T. L.; Buonsanti, R. $CsPbBr_3$ QD/AlO_x Inorganic Nanocomposites with Exceptional Stability in Water, Light, and Heat. *Angew. Chem. Int. Edit.* **2017,** *56*, 10696-10701.
(19) Sun, C.; Zhang, Y.; Ruan, C.; Yin, C. Y.; Wang, X. Y.; Wang, Y. D.; Yu, W. W. Efficient and Stable White LEDs with Silica-Coated Inorganic Perovskite Quantum Dots. *Adv. Mater.* **2016,** *28*, 10088-10094.
(20) Zhang, D. W.; Xu, Y.; Liu, Q. L.; Xia, Z. G. Encapsulation of $CH_3NH_3PbBr_3$ Perovskite Quantum Dots in MOF-5 Microcrystals as a Stable Platform for Temperature and Aqueous Heavy Metal Ion Detection. *Inorg. Chem.* **2018,** *57*, 4613-4619.
(21) Hou, S. C.; Guo, Y. Z.; Tang, Y. G.; Quan, Q. M. Synthesis and Stabilization of Colloidal Perovskite Nanocrystals by Multidentate Polymer Micelles. *ACS Appl. Mater. Inter.* **2017,** *9*, 18417-18422.
(22) Raja, S. N.; Bekenstein, Y.; Koc, M. A.; Fischer, S.; Zhang, D.; Lin, L.; Ritchie, R. O.; Yang, P.; Alivisatos, A. P. Encapsulation of Perovskite Nanocrystals into Macroscale Polymer Matrices: Enhanced Stability and Polarization. *ACS Appl. Mater. Inter.* **2016,** *8*, 35523-35533.
(23) Pan, A. Z.; Jurow, M. J.; Qiu, F.; Yang, J.; Ren, B. Y.; Urban, J. J.; He, L.; Liu, Y. Nanorod Suprastructures from a Ternary Graphene Oxide-Polymer-$CsPbX_3$ Perovskite Nanocrystal Composite That Display High Environmental Stability. *Nano Lett.* **2017,** *17*, 6759-6765.
(24) Pan, A. Z.; Wang, J. L.; Jurow, M. J.; Jia, M. J.; Liu, Y.; Wu, Y. S.; Zhang, Y. F.; He, L.; Liu, Y. General Strategy for the Preparation of Stable Luminous Nanocomposite Inks Using Chemically Addressable $CsPbX_3$ Peroskite Nanocrystals. *Chem. Mater.* **2018,** *30*, 2771-2780.
(25) Zhou, Q. C.; Bai, Z. L.; Lu, W. G.; Wang, Y. T.; Zou, B. S.; Zhong, H. Z. In Situ Fabrication of Halide Perovskite Nanocrystal-Embedded Polymer Composite Films with Enhanced Photoluminescence for Display Backlights. *Adv. Mater.* **2016,** *28*, 9163-9168.
(26) Aharon, S.; Wierzbowska, M.; Etgar, L. The Effect of the Alkylammonium Ligand's Length on Organic-Inorganic Perovskite Nanoparticles. *ACS Energy Lett.* **2018,** *3*, 1387-1393.
(27) Pan, J.; Quan, L. N.; Zhao, Y. B.; Peng, W.; Murali, B.; Sarmah, S. P.; Yuan, M. J.; Sinatra, L.; Alyami, N. M.; Liu, J. K.; Yassitepe, E.; Yang, Z. Y.; Voznyy, O.; Comin, R.; Hedhili, M. N.; Mohammed, O. F.; Lu, Z. H.; Kim, D. H.; Sargent, E. H.; Bakr, O. M. Highly Efficient Perovskite-Quantum-Dot Light-Emitting Diodes by Surface Engineering. *Adv. Mater.* **2016,** *28*, 8718-8725.
(28) Pan, J.; Shang, Y. Q.; Yin, J.; De Bastiani, M.; Peng, W.; Dursun, I.; Sinatra, L.; El-Zohry, A. M.; Hedhili, M. N.; Emwas, A. H.; Mohammed, O. F.; Ning, Z. J.; Bakr, O. M. Bidentate Ligand-Passivated $CsPbI_3$ Perovskite Nanocrystals for Stable Near-Unity Photoluminescence Quantum Yield and Efficient Red Light-Emitting Diodes. *J. Am. Chem. Soc.* **2018,** *140*, 562-565.
(29) Luo, B. B.; Pu, Y. C.; Lindley, S. A.; Yang, Y.; Lu, L. Q.; Li, Y.; Li, X. M.; Zhang, J. Z. Organolead Halide Perovskite Nanocrystals: Branched Capping Ligands Control Crystal Size and Stability. *Angew. Chem.*

Int. Edit. **2016,** *55*, 8864-8868.
(30) Huang, H.; Chen, B. K.; Wang, Z. G.; Hung, T. F.; Susha, A. S.; Zhong, H. Z.; Rogach, A. L. Water Resistant $CsPbX_3$ Nanocrystals Coated with Polyhedral Oligomeric Silsesquioxane and Their Use as Solid State Luminophores in All-perovskite White Light-emitting Devices. *Chem. Sci.* **2016,** *7*, 5699-5703.
(31) Zou, S. H.; Liu, Y. S.; Li, J. H.; Liu, C. P.; Feng, R.; Jiang, F. L.; Li, Y. X.; Song, J. Z.; Zeng, H. B.; Hong, M. C.; Chen, X. Y. Stabilizing Cesium Lead Halide Perovskite Lattice through Mn(II) Substitution for Air-Stable Light-Emitting Diodes. *J. Am. Chem. Soc.* **2017,** *139*, 11443-11450.
(32) Guria, A. K.; Dutta, S. K.; Das Adhikari, S.; Pradhan, N. Doping Mn^{2+} in Lead Halide Perovskite Nanocrystals: Successes and Challenges. *ACS Energy Lett.* **2017,** *2*, 1014-1021.
(33) Parobek, D.; Roman, B. J.; Dong, Y.; Jin, H.; Lee, E.; Sheldon, M.; Son, D. H. Exciton-to-Dopant Energy Transfer in Mn-Doped Cesium Lead Halide Perovskite Nanocrystals. *Nano Lett.* **2016,** *16*, 7376-7380.
(34) Zhu, J.; Yang, X.; Zhu, Y.; Wang, Y.; Cai, J.; Shen, J.; Sun, L.; Li, C. Room-Temperature Synthesis of Mn-Doped Cesium Lead Halide Quantum Dots with High Mn Substitution Ratio. *J. Phys. Chem. Lett.* **2017,** *8*, 4167-4171.
(35) Arunkumar, P.; Gil, K. H.; Won, S.; Unithrattil, S.; Kim, Y. H.; Kim, H. J.; Im, W. B. Colloidal Organolead Halide Perovskite with a High Mn Solubility Limit: A Step Toward Pb-Free Luminescent Quantum Dots. *J. Phys. Chem. Lett.* **2017,** *8*, 4161-4166.
(36) Huang, S. Q.; Li, Z. C.; Wang, B.; Zhu, N. W.; Zhang, C. Y.; Kong, L.; Zhang, Q.; Shan, A. D.; Li, L. Morphology Evolution and Degradation of $CsPbBr_3$ Nanocrystals under Blue Light-Emitting Diode Illumination. *ACS Appl. Mater. Inter.* **2017,** *9*, 7249-7258.
(37) Liu, Y.; Li, F.; Liu, Q.; Xia, Z. Synergetic Effect of Postsynthetic Water Treatment on the Enhanced Photoluminescence and Stability of $CsPbX_3$ (X = Cl, Br, I) Perovskite Nanocrystals. *Chem. Mater.* **2018**, *30*, 6922-6929
(38) Zhao, Z. F.; Wu, Z. H.; Cheng, J.; Jing, L.; Hou, Y. F. Nanocomposites of Perovskite Quantum Dots Embedded in Magnesium Silicate Hollow Spheres for Multicolor Display. *J. Phys. Chem. C* **2018,** *122*, 16887-16893.
(39) Malgras, V.; Henzie, J.; Takei, T.; Yamauchi, Y. Stable Blue Luminescent $CsPbBr_3$ Perovskite Nanocrystals Confined in Mesoporous Thin Films. *Angew. Chem. Int. Edit.* **2018,** *57*, 8881-8885.
(40) Dirin, D. N.; Protesescu, L.; Trummer, D.; Kochetygov, I. V.; Yakunin, S.; Krumeich, F.; Stadie, N. P.; Kovalenko, M. V. Harnessing Defect-Tolerance at the Nanoscale: Highly Luminescent Lead Halide Perovskite Nanocrystals in Mesoporous Silica Matrixes. *Nano Lett.* **2016,** *16*, 5866-5874.
(41) Malgras, V.; Tominaka, S.; Ryan, J. W.; Henzie, J.; Takei, T.; Ohara, K.; Yamauchi, Y. Observation of Quantum Confinement in Monodisperse Methylammonium Lead Halide Perovskite Nanocrystals Embedded in Mesoporous Silica. *J. Am. Chem. Soc.* **2016,** *138*, 13874-13881.
(42) Zhang, K.; Xu, L. L.; Jiang, J. G.; Calin, N.; Lam, K. F.; Zhang, S. J.; Wu, H. H.; Wu, G. D.; Albela, B.; Bonneviot, L.; Wu, P., Facile Large-Scale Synthesis of Monodisperse Mesoporous Silica Nanospheres with Tunable Pore Structure. *J. Am. Chem. Soc.* **2013,** *135*, 2427-2430.
(43) Di, X. X.; Jiang, J. T.; Hu, Z. M.; Zhou, L.; Li, P. Z.; Liu, S. J.; Xiang, W. D.; Liang, X. J. Stable and Brightly Luminescent All-inorganic Cesium Lead Halide Perovskite Quantum Dots Coated with Mesoporous Silica for Warm WLED. *Dyes Pigments* **2017,** *146*, 361-367.
(44) Chen, Y.; Yu, M. H.; Ye, S.; Song, J.; Qu, J. L. All-inorganic $CsPbBr_3$ Perovskite Quantum Dots Embedded in Dual-mesoporous Silica with Moisture Resistance for Two-photon-pumped Plasmonic Nano Lasers. *Nanoscale* **2018,** *10*, 6704-6711.
(45) Parobek, D.; Dong, Y. T.; Qiao, T.; Son, D. H. Direct Hot-Injection Synthesis of Mn-Doped $CsPbBr_3$ Nanocrystals. *Chem. Mater.* **2018,** *30*, 2939-2944.
(46) Cooke, G.; Rotello, V. M. Methods of Modulating Hydrogen Bonded Interactions in Synthetic Host-guest Systems. *Chem. Soc. Rev.* **2002,** *31*, 275-286.
(47) Yang, Y. W.; Sun, Y. L.; Song, N. Switchable Host-Guest Systems on Surfaces. *Accounts Chem. Res.* **2014,** *47*, 1950-1960.

(48) Liu, H. W.; Wu, Z. N.; Shao, J. R.; Yao, D.; Gao, H.; Liu, Y.; Yu, W. L.; Zhang, H.; Yang, B. $CsPb_xMn_{1-x}Cl_3$ Perovskite Quantum Dots with High Mn Substitution Ratio. *ACS Nano* **2017,** *11*, 2239-2247.
(49) Li, F.; Xia, Z. G.; Pan, C. F.; Gong, Y.; Gu, L.; Liu, Q. L.; Zhang, J. Z. High Br- Content $CsPb(Cl_yBr_{1-y})_{(3)}$ Perovskite Nanocrystals with Strong Mn2+ Emission through Diverse Cation/Anion Exchange Engineering. *ACS Appl. Mater. Inter.* **2018,** *10*, 11739-11746.
(50) Akkerman, Q. A.; D'Innocenzo, V.; Accornero, S.; Scarpellini, A.; Petrozza, A.; Prato, M.; Manna, L. Tuning the Optical Properties of Cesium Lead Halide Perovskite Nanocrystals by Anion Exchange Reactions. *J. Am. Chem. Soc.* **2015,** *137*, 10276-10281.
(51) Yang, D.; Cao, M.; Zhong, Q.; Li, P.; Zhang, X.; Zhang, Q. All-Inorganic Cesium Lead Halide Perovskite Nanocrystals: Synthesis, Surface Engineering and Applications. *J. Mater. Chem. C* **2019**, *7*, 757-789.
(52) Liu, W. Y.; Lin, Q. L.; Li, H. B.; Wu, K. F.; Robel, I.; Pietryga, J. M.; Klimov, V. I. Mn^{2+}-Doped Lead Halide Perovskite Nanocrystals with Dual-Color Emission Controlled by Halide Content. *J. Am. Chem. Soc.* **2016,** *138*, 14954-14961.